Implementation of a Long-Lasting, Untethered, Lightweight, Upper Limb Exoskeleton

Hao Liu, Kaiwen Fang, Leran Chen, Chenghao Xu, Cheng Chen, Ting Wang, Zining Wu, Gong Chen, Chenglong Fu, *Member, IEEE*, Jing Ye, and Hongqiang Wang, *Senior Member, IEEE*

***Abstract*—To prevent muscle fatigue or disorder due to long-term or repetitive arm-lifting in scenarios that heavily rely on manual operations, various exoskeletons have been developed previously. However, the exoskeletons with motors suffer from heavy mass and high cost, while previous passive exoskeletons possess poor adaptability to different arm angles, tasks, and users. To solve this problem, we designed a lightweight (3.1 kg) upper limb exoskeleton capable of providing a self-adaptable support force to the upper limbs based on linkage mechanisms and gas springs and a tunable maximum force (10–130 N) based on small motors and sensors. By altering the supporting angle and distance, the force curvature is adjustable by motors to adapt to the load in the hands. Since the motors adjust the dimension of the mechanical structure, instead of directly supporting the arms, the power consumption is low (1.85 W), and the exoskeleton operation duration is very long (11 h) using a 3000 mAh battery. The experimental results show that the measured surface electromyogram activities reduced up to 43.84% and 46.23% for static and dynamic tests, respectively.**

***Index Terms*—Linkage mechanism, mechanism design, metamorphic mechanism, physically assistive devices, wearable robots.**

Manuscript received 6 July 2023; revised 15 January 2024 and 23 April 2024; accepted 24 June 2024. Recommended by Technical Editor C. Chen and Senior Editor J. Ueda. This work was supported in part by the Natural Science Foundation of Guangdong Province of China under Grant 2024A1515010183, in part by the Science, Technology and Innovation Commission of Shenzhen Municipality under Grant ZDSYS20200811143601004, and in part by Guang dong Provincial Research Support Program under Grant 2019QN01Z733. *(Corresponding authors: Chenglong Fu; Jing Ye; Hongqiang Wang.)*

This work involved human subjects or animals in its research. Approval of all ethical and experimental procedures and protocols was granted by The Southern University of Science and Technology, Human participants Ethics Committee under Application No. 20210090, and performed in line with the Declaration of Helsinki.

Hao Liu is with the Shenzhen Key Laboratory of Biomimetic Robotics and Intelligent Systems, Southern University of Science and Technology, Shenzhen 518055, China.

Kaiwen Fang, Leran Chen, Cheng Chen, Ting Wang, and Zining Wu are with the Department of Mechanical and Energy Engineering, Southern University of Science and Technology, Shenzhen 518055, China.

Chenghao Xu is with IMOS Lab, Civil Engineering Department, EPFL, 1015 Lausanne, Switzerland.

Gong Chen and Jing Ye are with the Shenzhen MileBot Robotics Company, Ltd., Shenzhen 518055, China (e-mail: ye@milebot.com.cn).

Chenglong Fu is with the Shenzhen Key Laboratory of Biomimetic Robotics and Intelligent Systems, Southern University of Science and Technology, Shenzhen 518055, China, and also with the Guangdong Provincial Key Laboratory of Human-Augmentation and Rehabilitation Robotics in Universities, Southern University of Science and Technology, Shenzhen 518055, China (e-mail: fucl@sustech.edu.cn).

Hongqiang Wang is with the Shenzhen Key Laboratory of Biomimetic Robotics and Intelligent Systems, Department of Mechanical and Energy Engineering and Guangdong Provincial Key Laboratory of Human-Augmentation and Rehabilitation Robotics in Universities, Southern University of Science and Technology, Shenzhen 518055, China (e-mail: wanghq6@sustech.edu.cn).

This article has supplementary material provided by the authors and color versions of one or more figures available at https://doi.org/10.1109/TMECH.2024.3431884.

Digital Object Identifier 10.1109/TMECH.2024.3431884

Nomenclature

Name	Specification
ETL	The equivalent torso link (waist pivot to the shoulder joint).
EAL	The equivalent arm link (shoulder joint to the equivalent upper arm pivot).
RL	The rotary link of the exoskeleton.
VL	The vertical support link of the exoskeleton.
AC	The dotted line between A and C (see below).
A	The joint between RL and EAL.
B	The joint between VL and RL.
C	The joint between VL and ETL.
D	The joint between ETL and EAL.
E	The joint between the gas spring and the slider on VL.
F	The support force provided by the exoskeleton which is applied to the arm (normal to ground).
F_f	The friction force between RL and the slider on RL.
F_{gas}	The force of gas spring while working.
F_s	The spring force while working.
F_t	The compression force on the compression cycle test.
G	Total gravity (load) on the arm.
H	The joint between the gas spring and the slider on RL.
T	The adjuster.
a	Length of VL.
b	Length of RL.
c	Length of the ETL.
d	Length of the EAL.
e	Distance between B and E.
e_0	The initial length of e.
f	Max distance that the slider on RL can move from B.
f_{gas}	The friction force on the gas spring.
g	Length of gas spring while working.
g_m	The length parameter of the gas spring.
k	The spring ratio.
k_{gas}	The gas spring force coefficient.

n	Normalized parameter for variables.
x	The length of AC.
x_{f0}	The initial length of spring.
α	The angle between RL and AC.
β	The angle between VL and RL.
γ	The angle between ETL and EAL.
η	The angle between ETL and AC.
θ	The angle between RL and gas spring (on B side).
φ	The supplementary angle of θ.
φ_t	The transition angle of the exoskeleton.
σ	The acute angle between VL and gas spring.
μ	The friction force coefficient of the slider on RL.

I. Introduction

Although automation technologies boomed in the last decades, human–robot interaction has also improved [1], [2], [3], [4], [5], [6], manual operation still accounts for a large proportion of the industry and is indispensable due to the high customization and complexity of various tasks. Manual processes in working scenarios, such as automobile repair and interior decoration, usually involve arm-lifting while e.g., holding electric drills and forceps [7]. Lifting arms causes great pressure on workers' shoulders, arms, and back, leaving them fatigued in muscles and even causing severe upper limb disorders consequently after the long-term work [8], [9], [10]. Solutions are highly desired to improve manufacturing efficiency and ensure workers' health during the arm-lifting operation [11], [12].

The recent emerging technology of exoskeletons is a promising approach [13], [14], [15]. Inspired by insects, the exoskeleton can provide extra power to improve the users' performances in strength, speed, and endurance [16], [17]. Various passive exoskeleton structures have been developed and applied in the industry due to their lightweight, low-cost, and long operation period [18], [19], [20], [21], [22], [23], [24], [25]. Still, the poor adjustability and customization of the support force limits their applications. Although active exoskeletons can provide enough power amplification and more accurate motion augmentation for the users, most of the current active exoskeletons are bulky or tethered due to the power density limitation, which is inadequate for more extensive mobile applications [26], [27], [28], [29].

Is it possible to combine the advantages of both active and passive exoskeletons (being long-lasting, untethered, lightweight, self-adjustable, and low-cost)? Researchers have given us solutions to make semiactive exoskeletons [30], [31], [32], [33]. However, most of them have problems, such as being heavy, short-lasting time, minor in support force, and so on. To solve those problems, we implement a long-lasting, untethered, lightweight, upper limb exoskeleton by separating the force supporting and force adjustment to combine the advantages of passive and active exoskeletons.

In this exoskeleton, the support force is self-adjustable according to the arm lifting angle based on the passive energy storage mechanical structure, while the maximum support force is tunable according to the weight of the load based on the sensors and the small motors integrated into the exoskeleton. The exoskeleton developed in this work is long-lasting, untethered, and lightweight (3.1 kg), and the force changes spontaneously with the arm lift angle since we designed and synthesized a passive mechanical structure for the force support. Moreover, the maximum amplitude of the support force is automatically changed by a motor in a range from 10 to 130 N to adapt to the weight in hands when a radiofrequency identification device (RFID) module recognizes the object. Since the force for this adjustment is small, the motor is compact, and the energy consumption (1.85 W, lasted for 11 h in our test) and cost (135 USD) are both considerably low, which is suitable for more extensive applications requiring long-lasting, economical, and mobile assistance devices. With this exoskeleton, the participants' surface electromyogram (sEMG) activities can be reduced by up to 43.84% and 46.23% for static and dynamic tests, respectively, showing its great effective assistance to the users.

The rest of this article is organized as follows. Section II introduces the kinematics and dynamics modeling and synthesis of the mechanical structure of the exoskeleton. Section III focuses on the parametric analysis and optimization based on force balance models. The manufacture and assembly methods are explained in Section IV. Then, experiments are conducted to characterize the support force, metabolic expenditure, and electromyogram value. Finally, Section V concludes this article.

II. Mechanical Synthesis and Modeling

The shoulder has large mobility due to its complex skeletal structure and fewer constraints [34]. A global system is usually used to simplify the description in practical engineering studies [35]. In this article, we use this global system to describe the shoulder joints, and it can be simplified as three rotation Degrees of Freedom (DOFs) [36]. While the arm is moving downward, the exoskeleton should resist the gravity force of the arm and objects in hand while leaving the other two DOFs free. Therefore, to avoid the misalignment of the exoskeleton support joint and shoulder joint during movement, thereby reducing the discomfort, we used two passive ball joints to connect the exoskeleton support structure and the human body fixtures [37].

In our design, the classical four-bar linkage mechanism is employed to support the load, considering its low cost, simple structure, and lightweight [in Fig. 1(a) and (b), and Supplementary movie 1]. In this mechanism, the human upper torso and upper arm are regarded as two adjacent links of the four-bar linkage, and the exoskeleton as the other two links, as shown in Fig. 2(a). We mainly need to analyze and synthesize this mechanism for the vertical support force. The following analysis assumes that the equivalent body links and the exoskeleton links are all in the same 2-D vertical plane, which can be achieved with the help of the connecting string and the suspension ball joint.

To avoid disturbance or accidents, the exoskeleton links VL and RL (the meanings of all the parameters in this article can be found in Nomenclature) in Fig. 2(a) are expected to be placed outside of the angle between the links ETL and EAL, which satisfy

$$a > c, \quad b > d, \quad a > b. \tag{1}$$

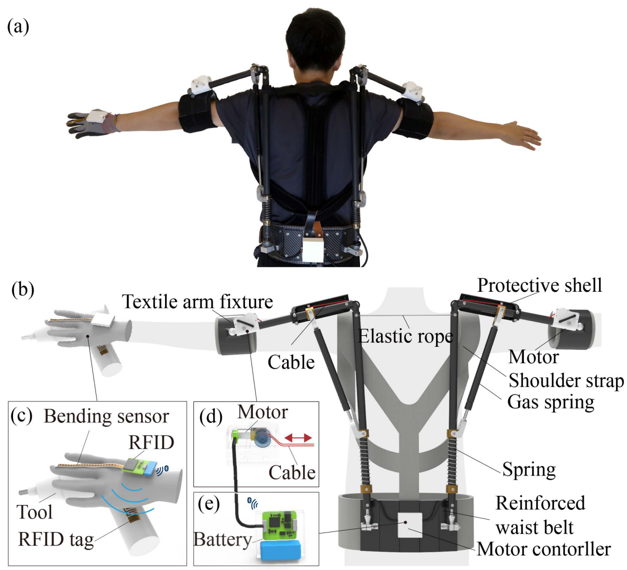

Fig. 1. Overall view of the upper limb exoskeleton. (a) Photograph of the exoskeleton. (b) Model of the exoskeleton. (c) Schematic of the RFID recognition module. (d) Schematic of the motor. (e) Schematic of the motor controller.

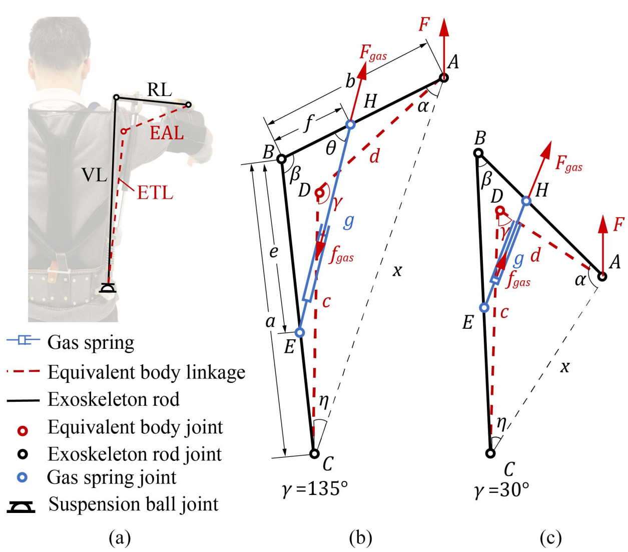

Fig. 2. Kinematic analysis for the exoskeleton mechanism. (a) Structure sketch of the four-bar linkage. Four-bar linkage supported by a gas spring under different arm postures. (b) $\gamma = 135°$. (c) $\gamma = 30°$.

For the free movement of the upper arm and to ensure the free movement of the shoulder, according to Grashof's law, we have

$$a + b > c + d, \quad a - b < c - d. \tag{2}$$

Based on the above-mentioned inequalities, the available values of a and b for men and women can be obtained by linear programming, as shown in Fig. 3(a). In the analysis, d ranges from 170 to 230 mm since the arm fixture is set at 2/3 of the upper arm, and the average length of the upper arm is 279–349 mm for adult men and 252–319 mm for adult women in China (height from 1.45–1.83 m) [38]. c ranges from 400–500 mm since the distance from the hip to the shoulder is between

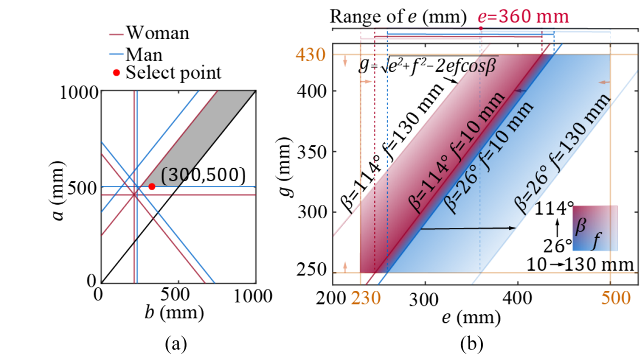

Fig. 3. Linear programming for the four-bar linkage. (a) Available ranges of a and b are shown in shaded gray areas. a = 500 mm and b = 300 mm are selected as the length of a and b, respectively, in this work. (b) Relationship between g and e for different β and f. The range of e is the intersection of the range of all the curves in the diagram.

432–502 mm and 403.5–459.5 mm for adult men and women, respectively [38]. Therefore, here a and b are selected as 500–300 mm, respectively, concerning the adaptability to extended body sizes and the compactness of the exoskeleton.

To provide a support force, we add a gas spring between the two exoskeleton links, as shown in Fig. 2(b) and (c). The gas spring is composed of a cylinder with compressed gas inside, and it can provide a relatively stable resisting force while subjected to a load. Based on the geometric diagram shown in Fig. 2(b) and (c), we have the following relationships:

$$\begin{cases} x^2 = a^2 + b^2 - 2ab\cos\beta \\ x^2 = c^2 + d^2 - 2cd\cos\gamma \\ g^2 = e^2 + f^2 - 2ef\cos\beta \\ a^2 = x^2 + b^2 - 2xb\cos\alpha \\ d^2 = c^2 + x^2 - 2cx\cos\eta \end{cases} \tag{3}$$

$$\frac{\sin\theta}{\sin\beta} = \frac{e}{g}, \quad \frac{\sin\beta}{\sin\alpha} = \frac{x}{a}, \quad \frac{\sin\eta}{\sin\gamma} = \frac{d}{x}. \tag{4}$$

According to previous literature [39], the main desired range of γ to support load is from 30° to 135°. The corresponding range of β is from 26° (assuming $c = 170$ mm, $d = 400$ mm) to 114° (assuming $c = 230$ mm, $d = 500$ mm) according to (3). We initially set the adjustable range of f [shown in Fig. 2(b) and (c)] from 10 to 130 mm, considering the compactness. Moreover, we primarily select a gas spring with a stroke of 180 mm (minimum length 250 mm, maximum length 430 mm) and a nominal force of 250 N [40] for the following analysis. Based on (3), we draw the $g - e$ diagram in Fig. 3(b), in which both f and β are variable, represented by different colors and transparencies. To ensure that the mechanism can work in the entire ranges of g, f, and β, we can select e as 360 mm.

Assuming the user is standing, ETL is vertical. According to the torque balance, the support force at Joint A is, as shown in Fig. 2(b) and (c)

$$F = F_{\text{gas}} \frac{f\sin\theta}{b\sin(\alpha + \eta)}. \tag{5}$$

According to (3) and (4), (5) can be transformed as

$$F = F_{\text{gas}} \frac{ef}{bd} \frac{1}{\sqrt{e^2 + f^2 - 2ef\cos\beta}} \frac{2cd\cos\gamma - c^2 - d^2}{a\sin\beta\cos\gamma + (a\cos\beta - b)\sin\gamma} \tag{6}$$

where

$$\beta = \arccos\left(\frac{a^2 + b^2 - c^2 - d^2 + 2cd\cos\gamma}{2ab}\right). \tag{7}$$

Based on (6), the support force is relatively constant for different values of γ.

Until now, the exoskeleton could provide a support force to the user's upper arms, but we still need the maximum force to be tunable, and the force is self-adaptable for the arm lift angle. For this purpose, we add a slider on the upper joint of the gas spring (Joint H). The position of this slider is limited by a cable, as shown in Fig. 4(b). An adjuster can shorten the length of the cable, and the corresponding support force on the arms reduces according to (6).

Here, we define two modes, supporting and relaxing mode, as shown in Fig. 4(a). When the angle φ is just to be smaller than 90°, the slider at Joint H spontaneously slips to Joint B (relaxing mode) due to the force balance, and the support force suddenly drops to a low level, allowing the arms to rest near its vertical posture. To reduce the impact of the sudden force change, another slider and spring are installed on Joint E.

The relationship between the support force and variables is calculated by force equilibrium. Spring force F_s applied on the spring is

$$F_s = F_{\text{gas}}\cos\sigma \tag{8}$$

where

$$\sigma = \arcsin\left(\frac{f\sin\beta}{\sqrt{e^2 + f^2 - 2ef\cos\beta}}\right). \tag{9}$$

The force on the gas spring can be simplified as a linear function

$$F_{\text{gas}} = \begin{cases} k_{\text{gas}}(g - g_m) - f_{\text{gas}}, & \text{upward} \\ k_{\text{gas}}(g - g_m) + f_{\text{gas}}, & \text{downward.} \end{cases} \tag{10}$$

According to Hooke's law

$$F_s = k(x_{f0} + e_0 - e) \tag{11}$$

where e_0 is 360 mm, x_{f0} is 100 mm. Based on (8) and (11), we can derive the value of F_{gas}

$$F_s = \mathcal{F}_s(f, \beta, k, x_{f0}, e_0). \tag{12}$$

According to lever law, we can achieve the support force F on the arm

$$F = F_{\text{gas}} \frac{f\sin\theta}{b\sin(\alpha + \eta)}. \tag{13}$$

Thus, we can calculate the support force F as

$$F = \mathcal{F}\left(f, \beta, a, b, c, d, k, x_{f0}, e_0\right). \tag{14}$$

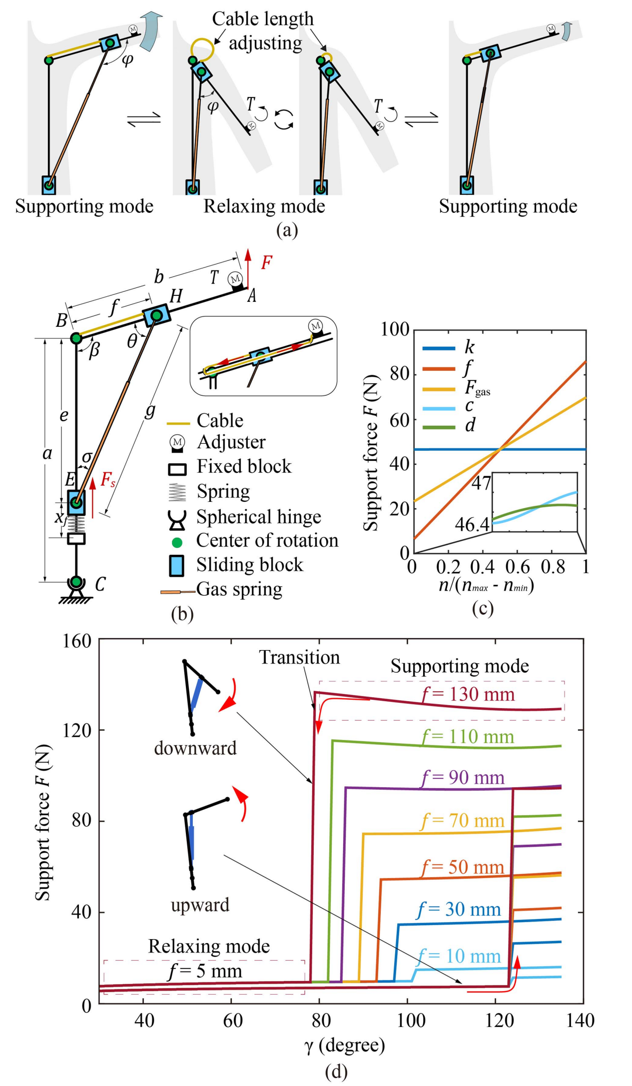

Fig. 4. Force analysis for the exoskeleton. (a) Diagram of the switch between supporting mode and relaxing mode. (b) Exoskeleton with sliders. F at Joint A represents the support force on the arm (the direction of F is parallel to ETL, which is not shown in this figure). (c) Support force F in angle $\gamma = 100°$ for normalized parameters n [e.g., $n = k$ / (maximum of k–minimum of k)]: the spring ratio k (3000–13 000 N/m), the maximum distance of upper copper bushing f (0.01–0.13 m), the gas spring force F_{gas} (100–300 N), the length of the ETL (c: 0.4–0.5 m), and the length of the EAL (d: 0.18–0.23 m). If not specified, the parameters are set as default values ($f = 70$ mm, $F_{\text{gas}} = 250$ N, $k = 7000$ N/m, $c = 470$ mm, $d = 210$ mm). (d) Mutation model of force for different f (the red dotted boxes represent the modes of $f = 130$ mm, $k_{\text{gas}} = -400$ N/m, $g_m = -1.075$ m, $f_{\text{gas}} = 40$ N).

III. Parameter Analysis and Optimization

In this section, we analyze the influences of the parameters in the supporting and relaxing modes as follows.

In the supporting mode, as shown in Fig. 4(c), for a specific arm lifting angle γ (100°), the spring ratio k, c, and d influence little on the support force, while the support force increases with the increase of f and F_{gas}. For an aimed support force, various sets of parameters can be selected.

When the exoskeleton switches between the two modes, the slider spontaneously slips. The transition angle φ_t (the outside angle between RL and the gas spring) is

$$\varphi_t = \begin{cases} \frac{\pi}{2} + \arctan\mu, & \text{upward} \\ \frac{\pi}{2} - \arctan\mu, & \text{downward.} \end{cases} \quad (15)$$

This angle is different for the upward and downward arm movements since the direction of the friction force is opposite. This difference benefits the operation since it allows more extensive ranges of supporting and relaxing modes for specific arm-moving directions.

Therefore, with the slider on the gas spring, the exoskeleton spontaneously transits between the relaxing mode and supporting mode according to the angle of the arm, as shown in Fig. 4(d). Besides, the support force in the supporting mode can be tuned by adjusting the max supporting distance f of the gas spring. For people with different body sizes, changing from supporting to relaxing mode happens at different arm-lifting angles. The smaller the user's height, the larger the arm-lifting angle when the transition occurs. Therefore, considering the actual working space for supporting mode, this exoskeleton is suitable for people with a height range from 1.6 to 1.83 m (supplementary movie 2 shows subjects with different heights (1.64, 1.74, and 1.83 m) wearing our exoskeletons, it worked well, and subjects did not feel particularly uncomfortable).

IV. Manufacture and Assembly

As shown in Fig. 1, the whole exoskeleton is symmetric for the middle vertical line. In the left/right half section of the exoskeleton, the main supporting links (corresponding to VL and RL in the model) were made by two carbon fiber tubes (T300, Φ 20 mm ∗ 16 mm) connected by a normal joint. The horizontal tube was connected to a textile arm fixture through a suspension ball joint to support the upper arm. Protective shells were added to it to prevent mechanical damage to the users. The vertical tube was installed on the reinforced waist belt by a ball joint. A gas spring (250–430 mm, 250 N) connected the middle of the two carbon fiber tubes with graphite copper bushings (Φ 30 mm ∗ 20 mm). The brushings can move freely on the tubes to work as sliders. Cables limit the brushing on the horizontal tube, and the length of the cables can be adjusted by a motor (CHIHAI MOTOR, CHF-GW12T-N20 VA ABHL, 0.6 W) to change the curvature of the support force. The replaceable pads on the inner side of the arm fixture and waist belt were made of soft mesh fabric, which can ensure comfort and breathability. Besides, the carbon fiber plates on the reinforced waist belt can disperse the force exerted on the waist by the exoskeleton.

An RFID module (Fangkang, UHF RFID Module) was attached to the glove, which could recognize different tools in hands by the RFID tag (Impinj M4E, ISO/IEC 18000-6 C EPC Class1 Gen2) attached on the tools. The tag can be easily glued on the tools (machinery) without any modification for the tools (machinery), and the information for the tools (machinery) needs to be imported into the tag through the exoskeleton recognition module in advance. A bending sensor (Flex sensor 4.5) is attached to the middle finger of the hand to sense the state of the hand, which can be used for manual control (Straightening or bending the fingers can control the increasing or decreasing of the support force, respectively). This module then sent the tool's information to the motor controller (Arduino Leonardo) by Bluetooth (CRS BC417), which drove the motor to adjust the support force to the corresponding value according to the tool's weight and the user's information (registered in the memory in advance. The user's information includes weight and height, the support force that compensates the user's arm weight can be calculated by that information), as shown in Fig. 1(c)–(e).

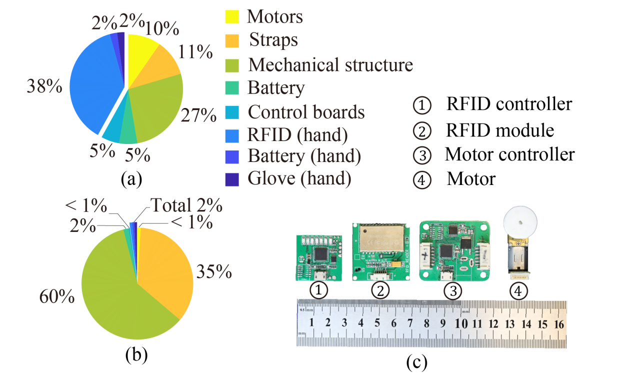

Fig. 5. Hardware information of the exoskeleton. (a) Cost distribution for the exoskeleton. (b) Weight distribution for the exoskeleton. (c) Photograph of the controller chips and motor.

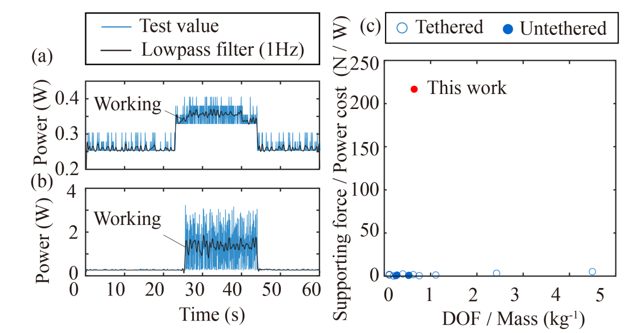

Fig. 6. Power of the (a) RFID recognition module and (b) motor control module for working and standby modes. (c) Comparison of different exoskeletons driven by motors [30], [41], [42], [43], [44], [45], [46], [47], [48], [49], [50], [51], [52], [53].

Because the motors are only used to control the length of cables rather than provide support for the arm directly, the automatic control system can be minimal in volume [see Fig. 5(c)] and ultralow in power consumption. The cable adjustment speed is 20 mm/s, and the average adjustment time on each side is about 2.5 s (assuming the cable length for each adjustment is 50 mm). As shown in Fig. 6, the power of RFID and motor control module are 0.35 and 1.5 W (power efficiency is 80%), respectively, which are powered by two lithium polymer batteries (DFRobot, 1000 mAh, 3.7 V, 0.5 A and ZONeSUN, 3000 mAh, 5 V, 2 A).

The overall mass of the passive exoskeleton is only 3.1 kg, while the part for the motors is only 0.03 kg. It can provide a support force to the upper arm up to 130 N. Compared with other active exoskeletons, our upper limb exoskeleton is lightweight, untethered, long-lasting, and ultralow in cost (only 135 USD due to the small motors.). The details of cost and weight distribution are shown in Fig. 5(a) and (b). To better evaluate the support

TABLE I
COMPARISON OF ACTIVE EXOSKELETONS

	Mass (kg)	support force (N)	Tethered	Actuator power (W)	Locations of application	Number of arms
Grazi et al. [30]	5	20	No	8	S	Two
Samper-escudero et al. [41]	0.89	130	Yes	>24	S+F	Two
Christensen et al. [42]	2.65	50	Yes	100	S+E	Right only
ExoSuit [43]	1.65	∼ 100	Yes	30	S+F	Two
Auxilio [44]	3.2	100	No	60	S+F	Right only
Kim et al. [45]	7.5	100	yes	100	S+E	Two
Zeiaee et al. [46]	7.66	177	Yes	260	S+E	Two
Xiloyannis et al. [54]	∼	28	∼	70	F	Left only
Sharma et al. [47]	7.5	<204	Yes	200	S+F	Right only
Kim et al. [48]	7.7	116	Yes	150	S+E	Left only
ARMin III [49]	18.76	125	Yes	90	S+E	Left only
Martinez et al. [50]	18.6	100	Yes	50	S+E	Right only
ULEL [55]	15.23	∼	Yes	>150	S+F+W	Right only
ULIX [51]	0.9	<33	Yes	>25	F	Left only
CRUX [56]	1.3	∼	No	∼	S+F	Two
Sui et al. [57]	4.2	∼	No	∼	S+E	Left only
Khan et al. [58]	∼	<150	Yes	∼	S+F	Right only
LIMPACT [52]	8	45	Yes	250	S+F	Right only
Buccelli et al. [53]	10	33	Yes	300	S+F	Right only
This work	3.1	130	No	0.6	S	Two

S: shoulder, F: forearm, E: elbow, W: wrist.

TABLE II
COMPARISON OF COMMERCIAL EXOSKELETONS

	Company	Weight (kg)	support force (N)	Adjustability	Time for donning and doffing (s)	Duration (h)
Airframe	Levitate Technologies Inc., USA	5	∼	∼	∼	∼
Eksoevo	Eksobionics,San Rafael, CA, USA	∼	22–68	Five levels	15–30	∼
ShoulderX [11]	SuitX, Emeryville, CA, USA	3.17	∼	∼	40	∼
MATE-XT [14]	Comau, Turin, Italy	3.5	∼	∼	30	∼
VEX [59]	Hyundai motor group, Korea	∼	13–29	Five levels	∼	∼
PAEXO [60]	Ottobock SE & Co. KGaA, Duderstadt, Germany	1.9	∼	∼	25	∼
MAPS-E	ULS Robotics, Shanghai, China	7.3	100	self-adaption	∼	6–8
H-PULSE	Pontedera, Italy	5	∼	self-adaption	∼	∼
This Work	∼	3.1	130	self-adaption	15–60	11

force, power, and weight performance of the exoskeleton, we make two indexes: the mass per DOF and the power consumption for a motor over a united exoskeleton support force on the hand (the torque of shoulder motor can be converted to the support force by dividing it with 0.3 m), to indicate the energy consumption and weight. As shown in Fig. 6(c) and Table I, our exoskeleton is much more lightweight and efficient than most industrial exoskeletons and exosuits [30], [41], [42], [43], [44], [45], [46], [47], [48], [49], [50], [51], [52], [53], [54], [55], [56], [57], [58]. Compared with other commercial exoskeletons (see Table II), our exoskeletons bridge the gap between active and passive exoskeletons while being lightweight and actively adjustable.

Work-related musculoskeletal disorders cause huge losses to the industry every year, and exoskeletons can reduce fatigue and disease occurrence, bringing huge economic benefits to enterprises. Due to our exoskeleton's superior support performance and the relatively low cost, there is a huge advantage in terms of cost-effectiveness and return on investment.

V. Experiment Verification

A. Characterization of the Gas Spring

The gas spring was characterized by a tensile testing machine (MTS Criterion Model 42) with a 500 mm/min loading speed. Although ideally, the resisting force of the gas spring is expected to be constant, in practice, it is not. As shown in Fig. 7(a), the gas spring force F_{gas} increases 30% during the compression process and reduces by approximately 21% when it recovers to the maximum length. The discrepancy is caused by the direction of the sliding friction force changing for the opposite movements.

B. Support Force Test

To measure the support force of the exoskeleton, as shown in Fig. 7(b), the main supporting unit was fixed on the tensile testing machine (MTS Criterion Model 42). The compression cycle tests were conducted at a 500 mm/min rate. For convenience, the length of f is adjusted by a manual device. Since the support force F is in a different direction from the compressing force F_t acquired through a load cell (MTS LSB.203) mounting on the moving stage, a delta transformation is used here

$$F = F_t(x)\frac{\sin\alpha}{\sin(\alpha+\eta)} \tag{16}$$

where $F_t(x)$ is the force recorded on the load cell.

As shown in Fig. 7(c), when the arm of the participant lays down from supporting mode, the support force changes from a large value (e.g., 130 N) to a small value (10 N) in the transition angle φ_t (where the corresponding angle γ is about 60°–80°,

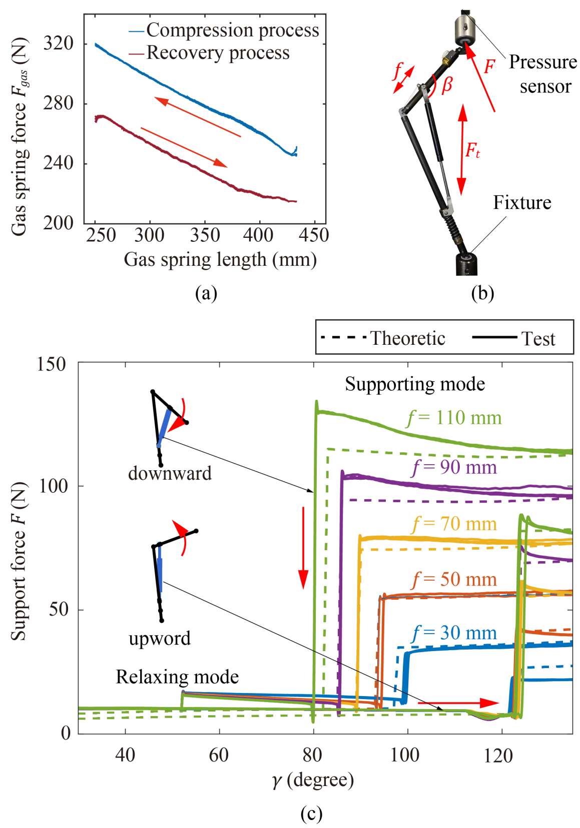

Fig. 7. Force experiment for the exoskeleton. (a) Gas spring force cycle test. (b) Experimental setup of the exoskeleton for the compression cycle test. (c) Theoretical and experimental force–angle curves of the exoskeleton with different lengths of f under compression cycles.

assuming c is 470 mm, and d is 210 mm.). On the contrary, when arms raise from the resting posture, the exoskeleton first generates a 10 N support force in response to assist the movement, and then transits to supporting mode until the angle γ larger than 120°. As predicted in the model, the transition angle φ_t is different for upward and downward processes (95° and 85°, respectively. This angle was acquired by assessing the video data of the transition process captured by a high-speed camera.) because of the friction force direction difference during these two processes.

Our mechanical model, including the force transition, is verified by the good agreement between experimental and theoretical results shown in Fig. 7(c). Moreover, as predicted in Section–III, the support force is adjustable by changing the magnitude of f. A larger support force is realized through a larger f. Besides, after decreasing the supporting distance f, the maximum support force decreases from 130 to 10 N. However, there are still some differences between theoretical and actual results. The reasons could be the exact mechanism of the exoskeleton-body system is not an ideal four-bar-linkage (e.g., the pivot offset in Joint E and Joint B, and the connection component between VL and gas spring is L-shape).

In our exoskeleton, the supporting distance was limited by the cable length, which was adjustable by the motors. Due to the weak load (less than 10 N) in relaxing mode, small motors

TABLE III
PARAMETERS IDENTIFICATION

Name	Value
Height	Measured by tapeline.
Weight	Measured by weight scale.
c	Weight $\times$ 27.6% [38].
d	Height $\times$ 18.4% $\times$ 2/3 [38].
F	Weight $\times$ 4.9% + weight of tool [61].
γ	90°.
f	Calculated by (14).

are available for this task, and the power consumption (mainly for the motors, control modules, and sensors) of the exoskeleton is considerably low. The motor, the control module, and the sensors generated the power consumption in the exoskeleton. The working time experiment shows that the exoskeleton lasted about 11 h until the 3000 mAh battery drained. The duration of the exoskeleton can be extended by simply replacing the battery in a few seconds.

C. Effectiveness

Four series of experiments, the rest state (RS) test, the Range of Motion (RoM) test, the static test, and the dynamic test, were performed to evaluate the supporting efficiency of the exoskeleton. None of the ten participants (24 ± 3 years old, weight at 74 ± 12 kg, and 178 ± 6 cm tall) had prior experience with any upper limb exoskeletons. Experiments were conducted by the Declaration of Helsinki. All participants were informed about the study's general purpose. All trials were approved by the Southern University of Science and Technology, Human Participants Ethics Committee (20210090), and consent was obtained from all participants.

The body parameters of the participants were obtained by measurement and calculation (see Table III), and the required support force was calculated when the angle between the subject's upper arm and torso was 90°.

The participants were randomly divided into two groups (group A and group B) to avoid the effect of the test order, and each group had five participants. Each test lasted 2 min and rested 10 min, thus reducing experimental errors due to fatigue. The experiment conditions were the same for each group except for the test order. For group A, the participants did the task with the exoskeleton first, then did the same task without the exoskeleton. The sequence of experiments in group B was reversed from that in group A.

1) RS Test: Each participant was asked to wear the exoskeleton and sit down to relax, with his arm up (supporting mode) and down (relaxing mode) for 2 min. For comparison, the sEMG signal was also measured for the participant in relaxed states without wearing the exoskeleton.

2) RoM Test: The participants wore the exoskeleton, carried no weight, and were asked to follow the trajectory of a marker for 2 min. The trajectory is in front of the participant, and the RoM of the experimenter's arm remained within 120° from left to right and 90° from up to down, as shown in Fig. 8(a). Then, the participants did the same task without wearing the exoskeleton.

This article has been accepted for inclusion in a future issue of this journal. Content is final as presented, with the exception of pagination.

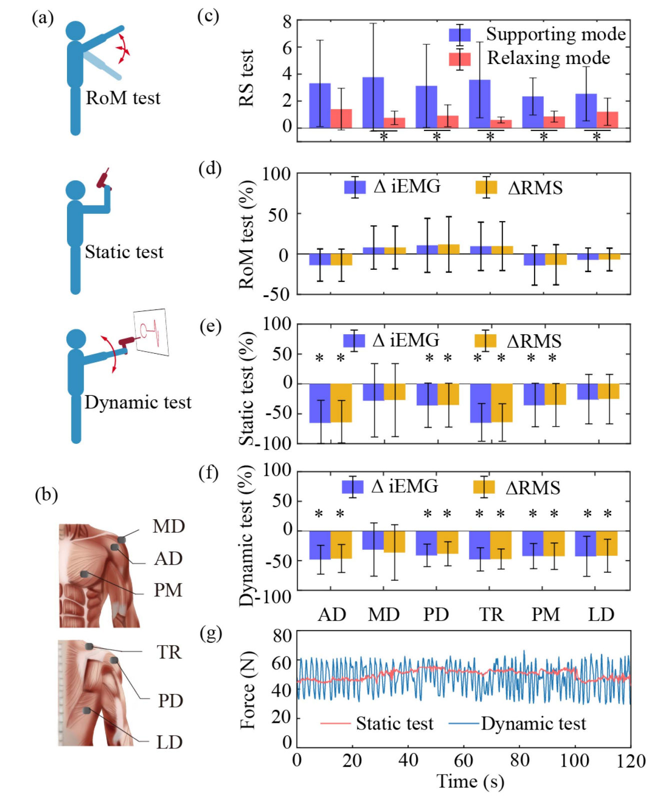

Fig. 8. sEMG test for the exoskeleton. Tested muscles included the AD, MD, PD, TR, PM, and LD. (a) Schematic diagram of RoM, static, and dynamic tests. (b) Schematic diagram of muscle electrode positions. (c) REA for different muscles under supporting and relaxing modes. (d) iEMG and rms signal result for RoM test. (e) iEMG and rms signal results for the static test. (f) iEMG and rms signal results for the dynamic tes t(*: $p < 0.05$.). (g) Support force F provided by the exoskeleton during static and dynamic tests for one person.

3) Static Lifting: Ten participants in group A were asked to hold a 2 kg drill overhead with one hand for 2 min by wearing the exoskeleton, and then hold the same drill by not wearing it after 10 min of interval rest. Group B has the opposite order. The angle between the torso and upper arm, upper arm, and lower arm were asked to keep around 90° during the test, as shown in Fig. 8(a).

4) Dynamic Load-Carrying: Ten participants held a 2 kg drill and were asked to follow the trajectory of a marker for 2 min. The trajectory was in front of the participant, and the center of it was at the same height as the eyes of the participant. The participants in group A did the task with the exoskeleton first and then held the same drill by not wearing it after 10 min of rest. Reversing the usual order, the participants in group B did the task without the exoskeleton first, then did the same task with the exoskeleton. The angle between the torso and upper arm for the participants should be around 90° during the test, as shown in Fig. 8(a).

The sEMG signal was obtained and analyzed for more practical applications to monitor muscle activation and evaluate the supporting performance during static and dynamic operations. The signal was collected by flexible electrode sEMG measuring instruments (Delsys, Trigno, wireless biofeedback system, USA). Six Trigno Avanti Wireless Sensors were attached to the anterior deltoid (AD), middle deltoid (MD), posterior deltoid (PD), TR, pectoralis major (PM) and latissimus dorsi (LD), respectively, to measure the sEMG signals, shown in Fig. 8(b)). The sampling rate is 1259 Hz. The sEMG signal was processed by a fourth order Butterworth band-pass filter (cutoff frequencies, 20–400 Hz), a fourth order Butterworth notch filter (cutoff frequency, 50 Hz), and a rectifier low-pass filter (zero-lag 100-ms moving average filter).

5) Statistics: Statistical analysis was used to determine the effect of the exoskeleton. The Shapiro–Wilk test ($\alpha = 0.05$) was used to assess the normality of the signals. The pairwise t-test (normal distribution) and the Wilcoxon signed-rank test (nonnormal distribution) were used to calculate the p-values.

6) Data Analysis: To verify the effect of the relaxing mode, the relative sEMG activity (REA) [integrated sEMG (iEMG) signal with the exoskeleton (in the position of supporting mode or relaxing mode) / integrated sEMG signal without the exoskeleton)] is calculated. For the static and dynamic test, ΔiEMG were calculated by the iEMG signal for the test with and without exoskeleton

$$\Delta\text{iEMG} = \left(\frac{\text{iEMG}_{\text{WE}} - \text{iEMG}_{\text{WOE}}}{\text{iEMG}_{\text{WOE}}}\right) \times 100\% \tag{17}$$

where $_{\text{WE}}$ and $_{\text{WOE}}$ means with and without the help of the exoskeleton, respectively. ΔRMS were calculated by the root-mean-square (rms) sEMG signal for the test with and without exoskeleton

$$\Delta\text{RMS} = \left(\frac{\text{RMS}_{\text{WE}} - \text{RMS}_{\text{WOE}}}{\text{RMS}_{\text{WOE}}}\right) \times 100\%. \tag{18}$$

Results of REA at RS were reported in Fig. 8(c). The participants with the exoskeleton in supporting mode have higher relative EMG activity (for AD, the comparison of the supporting mode and relaxing mode has a p-value larger than 0.05, while the p-values for other groups of muscles are smaller than 0.05) compared with participants with exoskeleton in relaxing mode. The result shows that wearing an exoskeleton to maintain a raised arm can also cause muscle fatigue, even if no external load is applied. Switching the exoskeleton to a relaxing mode can significantly reduce muscle fatigue caused by the lifted arm.

The results for the RoM test are shown in Fig. 8(d). The ΔiEMG and the ΔRMS in all the muscles have no statistically significant differences ($p > 0.05$) compared with 0, which means the exoskeleton did not affect the users' motion when the supporting level is minimum.

The results for the static and dynamic load-carrying test are shown in Fig. 8(e) and (f). The ΔiEMG and the ΔRMS in the static test for AD, PD, TR, and PM have a significant decrease ($p < 0.05$) compared with 0. The ΔiEMG and the ΔRMS in the dynamic test for AD, PD, TR, PM, and LD significantly decrease ($p < 0.05$) compared with 0. In total, the average ΔiEMG for all the muscles are –43.84% and –46.23% for static and dynamic tests, respectively, and the average ΔRMS for all the muscles are –43.42% and –42.40% for the static and dynamic test, respectively.

Fig. 8(g) shows the support force on a participant's arm (height: 1.74 m, weight: 68 kg) during dynamic and static tests. In the dynamic test, the support force on the arm is not constant but varies between 40 and 60 N. On the one hand, because of the difference in the support force during lifting and lowering the arm due to the friction. The other is due to the acceleration of the arm. The support force agrees with the theoretical calculation results during the static test.

VI. Discussion

In this article, we design a long-lasting, untethered, lightweight, upper limb exoskeleton that can increase the working efficiency for specific tool-based scenarios. For the kinematics of the exoskeleton, we suppose the four linkages are in the same plane. However, it is not in the actual situation due to the volume of the shoulder. The error is acceptable because the angle between the two planes (the plane of VL and RL, and the plane of ETL and EAL) is small. The support force of the exoskeleton in supporting mode is not constant but increases as the arm angle decreases. The users may consume more energy to overcome the excessive support force.

There are some limitations to the exoskeletons. First, the RFID can only recognize the tool with the tag. Specific tools need to be labeled before different tasks, which may limit the working scenarios of the exoskeleton. Second, the support force can only change under the relaxing mode due to the low power of the motor. Thus, the exoskeleton may not be suitable for working scenarios requiring frequent support force changes. Currently, the exoskeleton model does not consider the effect of the posture of the lower arm on the required support, which may result in inaccurate support force. Besides, although the adjustment time for the support force is about 2.5 s for each side of the exoskeleton, which is shorter than the adjustment time by hand adjustment, it is a relatively long time for the actual working environment. Our exoskeleton can significantly reduce the activity of the muscles in the shoulder (e.g., AD and TR), but it has less impact on the muscle activity of the LD, so the risk of injury from long-term arm lifting work still exists. Besides, some participants feel discomfort after long contact with the exoskeleton's waist belt and arm fixture.

VII. Conclusion

In this article, an efficient upper limb exoskeleton with adjustable force is modeled, designed, and fabricated based on a mechanical structure for passive arm support and motors for active tuning of the maximum support force. This untethered, long-lasting (11 h), lightweight (3.1 kg) upper limb exoskeleton is experimentally characterized and verified. Besides, the supporting performances of the exoskeleton under static and dynamic operations are evaluated through sEMG signal analysis. The sEMG activities for the upper arm were reduced by up to 43.84% and 46.23% for static and dynamic tests, respectively.

In the future, the components and materials can be further optimized for lighter weight, such as customized sliders and gas springs made from carbon fiber materials. The automatic control system can be more versatile by integrating, e.g., speech control, visual control, artificial intelligence control, and electroencephalogram control, to fit more working scenarios automatically and accelerate the application of the exoskeleton in industries. We can also add health monitoring systems to remind users to avoid long-term working. Moreover, sensors can be added to the lower arm to monitor its posture during the support force calculation. Furthermore, new mechanical designs or control methods can be added to expand the exoskeleton's working range from arm-lifting to all upper arm working scenarios. Besides, our exoskeleton will be rigorously tested in a real-world working environment in the future.

References

[1] T. B. Sheridan, "Human-robot interaction: Status and challenges," *Hum. Factors*, vol. 58, no. 4, pp. 525–532, 2016.

[2] S. Lemaignan et al., "Artificial cognition for social human-robot interaction: An implementation," *Artif. Intell.*, vol. 247, pp. 45–69, 2017.

[3] S. Bu, L. Yan, X. Gao, P. Zhao, and C. K. Lim, "Vision-guided manipulator operating system based on CSRT algorithm," *Int. J. Hydromechatronics*, vol. 5, no. 3, pp. 260–274, 2022.

[4] J. Dai and D. Caldwell, "Origami-based robotic paper-and-board packaging for food industry," *Trends Food Sci. Technol.*, vol. 21, no. 3, pp. 153–157, 2010.

[5] Y. Hu, N. Abe, M. Benallegue, N. Yamanobe, G. Venture, and E. Yoshida, "Toward active physical human-robot interaction: Quantifying the human state during interactions," *IEEE Trans. Hum. Mach. Syst.*, vol. 52, no. 3, pp. 367–378, Jun. 2022.

[6] Q. Xiong, X. Liang, and D. Wei, "So-EAGlove: VR haptic glove rendering softness sensation with force-tunable electrostatic adhesive brakes," *IEEE Trans. Robot.*, vol. 38, no. 6, pp. 3450–3462, Dec. 2022.

[7] X. Zhou and L. Zheng, "Model-based comparison of passive and active assistance designs in an occupational upper limb exoskeleton for overhead lifting," *IISE Trans. Occup. Ergon. Hum. Factors.*, vol. 9, no. 3–4, pp. 167–185, 2021.

[8] C. Latella et al., "Analysis of human whole-body joint torques during overhead work with a passive exoskeleton," *IEEE Trans. Hum. Mach. Syst.*, vol. 52, no. 6, pp. 1060–1068, Oct. 2022.

[9] M. F. Antwi-Afari et al., "Assessment of a passive exoskeleton system on spinal biomechanics and subjective responses during manual repetitive handling tasks among construction workers," *Saf. Sci.*, vol. 142, 2021, Art. no. 105382.

[10] M. A. Gull, T. Bak, and S. Bai, "Dynamic modeling of an upper limb hybrid exoskeleton for simulations of load-lifting assistance," *Proc. Inst. Mech. Eng. C. J. Mech. Eng. Sci.*, vol. 236, no. 5, pp. 2147–2160, 2022.

[11] L. Van Engelhoven et al., "Evaluation of an adjustable support shoulder exoskeleton on static and dynamic overhead tasks," in *Proc. Hum. Factors Ergonom. Soc. Annu. Meeting*, 2018, pp. 804–808.

[12] S. Yun et al., "Soft pneumatic elbow exoskeleton reduces the muscle activity, metabolic cost and fatigue during holding and carrying of loads," *Sci. Robot.*, vol. 6, no. 57, 2021, Art. no. eabe1243.

[13] M. Cempini, T. Cortese, and N. Vitiello, "A comparison between three commercially available exoskeletons in the automotive industry: An electromyographic pilot study," *J. Neuroeng. Rehabil.*, vol. 15, no. 1, pp. 1–13, 2018.

[14] I. Pacifico et al., "An experimental evaluation of the proto-MATE: A novel ergonomic upper-limb exoskeleton to reduce workers' physical strain," *IEEE Robot. Automat. Mag.*, vol. 27, no. 1, pp. 54–65, Mar. 2020.

[15] S. Lee et al., "Biomechanical and metabolic effectiveness of an industrial exoskeleton for overhead work," *Int. J. Ind. Ergon.*, vol. 80, 2020, Art. no. 102917.

[16] H. Choi, B. B. Kang, B.-K. Jung, and K.-J. Cho, "Exo-wrist: A soft tendon-driven wrist-wearable robot with active anchor for dart-throwing motion in hemiplegic patients," *IEEE Robot. Autom. Lett.*, vol. 4, no. 4, pp. 4499–4506, Oct. 2019.

[17] F. Parietti and H. Asada, "Supernumerary robotic limbs for human body support," *IEEE Trans. Robot.*, vol. 32, no. 2, pp. 301–311, Apr. 2016.

[18] R. Altenburger et al., "Design of a passive, iso-elastic upper limb exoskeleton for gravity compensation," *Robomech J.*, vol. 3, no. 1, pp. 1–7, 2016.

[19] T. Bosch et al., "The effects of a passive exoskeleton on muscle activity, discomfort and endurance time in forward bending work," *Appl. Ergon.*, vol. 54, pp. 212–217, 2016.
[20] K. Huysamen et al., "Evaluation of a passive exoskeleton for static upper limb activities," *Appl. Ergon.*, vol. 70, pp. 148–155, 2018.
[21] M. Pillai, L. Van Engelhoven, and H. Kazerooni, "Evaluation of a lower leg support exoskeleton on floor and below hip height panel work," *Hum. Factors*, vol. 62, no. 3, pp. 489–500, 2020.
[22] S. Iranzo, A. Piedrabuena, D. Iordanov, U. Martinez-Iranzo, and J.-M. Belda-Lois, "Ergonomics assessment of passive upper-limb exoskeletons in an automotive assembly plant," *Appl. Ergonom.*, vol. 87, 2020, Art. no. 103120.
[23] J. P. Pinho and A. Forner-Cordero, "Shoulder muscle activity and perceived comfort of industry workers using a commercial upper limb exoskeleton for simulated tasks," *Appl. Ergonom.*, vol. 101, 2022, Art. no. 103718.
[24] A. Blanco, J. M. Catalán, D. Martínez-Pascual, J. V. García-Pérez, and N. García-Aracil, "The effect of an active upper-limb exoskeleton on metabolic parameters and muscle activity during a repetitive industrial task," *IEEE Access*, vol. 10, pp. 16479–16488, 2022.
[25] M. W. Watterworth, R. Dharmaputra, R. Porto, J. A. Cort, and N. J. L. Delfa, "Equations for estimating the static supportive torque provided by upper-limb exoskeletons," *Appl. Ergonom.*, vol. 113, 2023, Art. no. 104092.
[26] H.-C. Hsieh, D.-F. Chen, L. Chien, and C. -C. Lan, "Design of a parallel actuated exoskeleton for adaptive and safe robotic shoulder rehabilitation," *IEEE/ASME Trans. Mechatron.*, vol. 22, no. 5, pp. 2034–2045, Oct. 2017.
[27] Y. Wang, A. Zahedi, Y. Zhao, and D. Zhang, "Extracting human-exoskeleton interaction torque for cable-driven upper-limb exoskeleton equipped with torque sensors," *IEEE/ASME Trans. Mechatron.*, vol. 27, no. 6, pp. 4269–4280, Dec. 2022.
[28] P. Xiang, L. Yan, Y. Guo, X. He, C. Gerada, and I.-M. Chen, "A concentrated-flux-type PM machine with irregular magnets and iron poles," *IEEE/ASME Trans. Mechatron.*, vol. 29, no. 1, pp. 691–702, Feb. 2024.
[29] R. Gopura et al., "Developments in hardware systems of active upper-limb exoskeleton robots: A review," *Rob. Auton. Syst.*, vol. 75, pp. 203–220, 2016.
[30] L. Grazi, E. Trigili, G. Proface, F. Giovacchini, S. Crea, and N. Vitiello, "Design and experimental evaluation of a semi-passive upper-limb exoskeleton for workers with motorized tuning of assistance," *IEEE Trans. Neural Syst. Rehabil. Eng.*, vol. 28, no. 10, pp. 2276–2285, Oct. 2020.
[31] S. H. Lee et al., "Evaluation of a novel active exoskeleton for tasks at or above head level," *Appl. Ergon.*, vol. 73, pp. 150–157, 2018.
[32] A. M. Saberi, N. Moser, and D. B. Popovi'c, "Kinematics-based adaptive assistance of a semi-passive upper-limb exoskeleton for workers in static and dynamic tasks," *J. Neuroeng. Rehabil.*, vol. 17, no. 1, pp. 1–18, 2020.
[33] K. Chua et al., "Unobtrusive, natural support control of an adaptive industrial exoskeleton using force myography," *J. Neuroeng. Rehabil.*, vol. 16, no. 1, pp. 1–12, 2019.
[34] D. Haering, M. Raison, and M. Begon, "Measurement and description of three-dimensional shoulder range of motion with degrees of freedom interactions," *J. Biomechanical Eng.*, vol. 136, no. 8, 2014, Art. no. 084502.
[35] C. A. Doorenbosch, J. Harlaar, and D. Veeger, "The globe system: An unambiguous description of shoulder positions in daily life movements," *J. Rehabil. Res. Develop.*, vol. 40, no. 2, pp. 147–155, 2003.
[36] C. J. van Andel et al., "Complete 3D kinematics of upper extremity functional tasks," *Gait Posture*, vol. 27, no. 1, pp. 120–127, 2008.
[37] D. Galinski, J. Sapin, and B. Dehez, "Optimal design of an alignment-free two-dof rehabilitation robot for the shoulder complex," in *Proc. IEEE 13th Int. Conf. Rehabil. Robot.*, 2013, pp. 1–7.
[38] CNIS, "GB 10000-88: Human dimensions of chinese adults," SAMR, Tech, Rep., 1988.
[39] A. de Vries et al., "The amount of support provided by a passive arm support exoskeleton in a range of elevated arm postures," *IISE Trans. Occup. Ergon. Hum. Fact.*, vol. 7, no. 3/4, pp. 311–321, 2019.
[40] D. Zhi et al., "GB/T 39433-2020: Gas spring design calculation," SAMR, 2020.
[41] J. L. Samper-Escudero, A. Giménez-Fernández, and Á. Gil-Agudo, "A cable-driven exosuit for upper limb flexion based on fibres compliance," *Sensors*, vol. 20, no. 16, 2020, Art. no. 4462.
[42] S. Christensen and S. Bai, "Kinematic analysis and design of a novel shoulder exoskeleton using a double parallelogram linkage," *J. Mech. Robot.*, vol. 10, no. 4, 2018, Art. no. 041008.
[43] M. Hosseini, R. Meattini, A. San-Millan, G. Palli, C. Melchiorri, and J. Paik, "A sEMG-driven soft exosuit based on twisted string actuators for elbow assistive applications," *IEEE Robot. Autom. Lett.*, vol. 5, no. 3, pp. 4094–4101, Jul. 2020.
[44] I. Gaponov et al., "Auxilio: A portable cable-driven exosuit for upper extremity assistance," *Int. J. Control Autom. Syst.*, vol. 15, no. 1, pp. 73–84, 2017.
[45] Y. G. Kim et al., "A voice activated bi-articular exosuit for upper limb assistance during lifting tasks," *Comput. Integr. Manuf.*, vol. 66, 2020, Art. no. 101995.
[46] A. Zeiaee et al., "Design and kinematic analysis of a novel upper limb exoskeleton for rehabilitation of stroke patients," in *Proc. IEEE Int. Conf. Rehabil. Robot.*, 2017, pp. 759–764.
[47] M. K. Sharma et al., "Design and fabrication of an intention based upper-limb exo-skeleton," in *Proc. IEEE Int. Symp. Ind. Electron.*, 2016, pp. 1–6.
[48] J.-Y. Kim et al., "Design, motion planning and control of frozen shoulder rehabilitation robot," *Int. J. Precis. Eng. Manuf.*, vol. 15, no. 9, pp. 1875–1881, 2014.
[49] T. Nef et al., "ARMin III–arm therapy exoskeleton with an ergonomic shoulder actuation," *Appl. Bionics Biomech.*, vol. 6, no. 2, pp. 127–142, 2009.
[50] F. Martinez et al., "Design of a five actuated DoF upper limb exoskeleton oriented to workplace help," in *2nd IEEE RAS EMBS Int. Conf. Biomed. Robot. Biomechatronics*, 2008, pp. 169–174.
[51] T. Chen, R. Casas, and P. S. Lum, "An elbow exoskeleton for upper limb rehabilitation with series elastic actuator and cable-driven differential," *IEEE Trans. Robot.*, vol. 35, no. 6, pp. 1464–1474, Dec. 2019.
[52] A. Otten, C. Voort, A. Stienen, R. Aarts, E. van Asseldonk, and H. van der Kooij, "LIMPACT: A hydraulically powered self-aligning upper limb exoskeleton," *IEEE/ASME Trans. Mechatron.*, vol. 20, no. 5, pp. 2285–2298, Oct. 2015.
[53] S. Buccelli et al., "A gravity-compensated upper-limb exoskeleton for functional rehabilitation of the shoulder complex," *Appl. Sci.*, vol. 12, no. 7, 2022, Art. no. 3364.
[54] M. Xiloyannis et al., "Physiological and kinematic effects of a soft exosuit on arm movements," *J. Neuroeng. Rehabil.*, vol. 16, no. 1, pp. 1–15, 2019.
[55] T. Madani, B. Daachi, and K. Djouani, "Modular-controller-design-based fast terminal sliding mode for articulated exoskeleton systems," *IEEE Trans. Control Syst. Technol.*, vol. 25, no. 3, pp. 1133–1140, May 2017.
[56] S. Lessard, P. Pansodtee, A. Robbins, J. M. Trombadore, S. Kurniawan, and M. Teodorescu, "A soft exosuit for flexible upper-extremity rehabilitation," *IEEE Trans. Neural Syst. Rehabil. Eng.*, vol. 26, no. 8, pp. 1604–1617, Aug. 2018.
[57] D. Sui et al., "Design of a wearable upper-limb exoskeleton for activities assistance of daily living," in *Proc. IEEE/ASME Int. Conf. Adv. Intell. Mechatron.*, 2017, pp. 845–850.
[58] A. M. Khan et al., "Passivity based adaptive control for upper extremity assist exoskeleton," *Int. J. Control Autom. Syst.*, vol. 14, no. 1, pp. 291–300, 2016.
[59] Y.-K. Kong, J. H. Kim, H.-H. Shim, J.-W. Shim, S.-S. Park, and K.-H. Choi, "Efficacy of passive upper-limb exoskeletons in reducing musculoskeletal load associated with overhead tasks," *Appl. Ergonom.*, vol. 109, 2023, Art. no. 103965.
[60] C. Latella et al., "Analysis of human whole-body joint torques during overhead work with a passive exoskeleton," *IEEE Trans. Human-Mach. Syst.*, vol. 52, no. 5, pp. 1060–1068, Oct. 2022.
[61] C. E. Clauser, J. T. Mc Conville, and J. W. Young, "Weight, volume, and center of mass of segments of the human body," *Nat. Tech. Inf. Service*, Springfield, VA,USA, 1969.

Hao Liu received the B.S. degree in mechanical engineering from the Southern University of Science and Technology, Shenzhen, China, in 2020. He is currently working toward the Ph.D. degree in intelligent manufacturing and robotics with the Department of Mechanical and Energy Engineering, Southern University of Science and Technology.

His research interests include soft robotics, microrobotics, bionic robotics, and advanced actuators.

Kaiwen Fang received the B.S. degree in robotic engineering from the Southern University of Science and Technology, Shenzhen, China, in 2021. He is currently working toward the M.S. degree in intelligent manufacturing and robotics with the Department of Mechanical and Energy Engineering, Southern University of Science and Technology.

His research interests include deep learning, computer vision, and physical simulation.

Leran Chen received the B.S. degree in mechanical engineering from the Southern University of Science and Technology (SUSTech), Shenzhen, China, in 2020, where he is currently working toward the Ph.D. degree in industrial engineering in the collaborate Ph.D. program between SUSTech and Hong Kong Polytechnic University, Hong Kong.

His research interests include machine learning, customized algorithms, and smart manufacturing.

Chenghao Xu received the B.Eng. degree in mechanical engineering from the Southern University of Science and Technology, Shenzhen, China, in 2020, and the M.Sc. degree in robotics from the Delft University of Technology, Delft, The Netherlands, in 2023. He is currently working toward the Ph.D. degree in 3D vision and robot perception with EPFL, Lausanne, Switzerland.

His research interests include robot perception, visual SLAM, and 3-D vision.

Cheng Chen received the B.S. degree in mechanical engineering from the University of Electronic Science and Technology, Chengdu, China, in 2019, and the Ph.D. degree in biomedical engineering from the National University of Singapore, Singapore, in 2024.

He is currently a Research Fellow with the Department of Mechanical and Energy Engineering, Southern University of Science and Technology, Shenzhen, China. His research interests include soft robotics and variable stiffness.

Ting Wang received the B.S. degree in mechanical design and manufacturing and automation from Southwest Jiaotong University, Chengdu, China, in 2013, and the M.S. degree in mechanical and electronical engineering from the Huazhong University of Science and Technology, Wuhan, China, in 2016. She is currently working toward the Ph.D. degree in biomedical engineering with the Department of Mechanical and Energy Engineering, Southern University of Science and Technology, Shenzhen, China, and the Department of Biomedical Engineering, City University of Hong Kong, Hong Kong.

Her research interests include microrobotics, bioinspired robotics, advanced actuators, flapping-wing robots, microaerial vehicles, and medical robotics.

Zining Wu is currently working toward the B.S. degree in robot engineering with the Department of Mechanical and Energy Engineering, Southern University of Science and Technology, Shenzhen, China.

His research interests include soft robotics, electrostatic film robotics, bionic robotics, and robotic exoskeletons.

Gong Chen received the B.S. degree in mechanical engineering & automation from the Department of Mechanical and Power Engineering, Shanghai Jiao Tong University, Shanghai, China, in 2011, and the Ph.D. degree in biomedical engineering from the Department of Biomedical Engineering, National University of Singapore, Singapore, in 2016.

His research interests include rehabilitation robot systems, new robot drivers, and human–computer interactive control.

Chenglong Fu (Member, IEEE) received the B.S. degree in mechanical engineering and automation from the Department of Mechanical Engineering, Tongji University, Shanghai, China, in 2002, and the Ph.D. degree in mechatronic engineering from the Department of Precision Instruments and Mechanology, Tsinghua University, Beijing, China, in 2007.

He is currently a Professor with the Department of Mechanical and Energy Engineering, Southern University of Science and Technology, Shenzhen, China. His research interests include dynamic walking, biped and humanoid robots, powered prosthesis, lower limb exoskeleton, and human–robot interaction.

Jing Ye received the Ph.D. degree in biomedical engineering from the Waseda University, Shinjuku, Japan, in 2015.

His research interests include medical rehabilitation robots, mobile robot systems, and minimally invasive surgical robots.

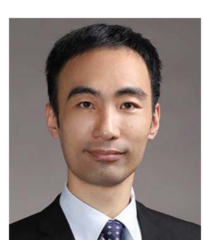

Hongqiang Wang (Senior Member, IEEE) received the B.S. and M.S. degrees in mechanical engineering from the Xi'an Jiao Tong University, Xi'an, China, in 2008 and 2011, respectively, and the Ph.D. degree in precision mechanical engineering from Tokyo University, Tokyo, Japan, in 2015.

He is currently an Associate Professor with the Department of Mechanical and Energy Engineering, Southern University of Science and Technology, Shenzhen, China. His research interests include miniature robotics, novel actuators, new flexible motors, soft robotics, and medical robotics.